DOI: 10.1002/anie.200904877

Cluster Formation

# Spectroscopic Elucidation of First Steps of Supported Bimetallic Cluster Formation**

*Apoorva Kulkarni and Bruce C. Gates**

Supported bimetallics are among the most important industrial catalysts, with applications for example in petroleum naphtha reforming and automobile exhaust conversion.[1] Industrial bimetallic catalysts typically consist of high-area oxide supports with particles of metal dispersed on them—particles of various compositions, shapes, and sizes, ranging from small clusters to particles large enough to be metallic.[2] In a typical preparation, a support such as $\gamma$-$Al_2O_3$ is brought in contact with an aqueous solution of precursor salts, and the resultant material is dried and treated with $H_2$ at a temperature high enough to reduce the metals. The cluster synthesis has parallels with cluster formation in solution,[3] but the initial steps are only beginning to be understood.[4] There is substantial evidence of monometallic cluster formation,[3] but little is known about bimetallic cluster formation.

Because not all of the supported species in these catalysts are bimetallic, researchers have alternatively used organometallic clusters with heterometallic bonds as precursors on the supports, followed by activation to remove ligands from the cluster frame. This approach is limited, however, because the activation often leads to undesired fragmentation and/or aggregation of the metal, typically with loss of uniformity of the metal frames, so that the final structures may hardly be distinguishable from those of conventionally prepared catalysts.

Our goal was to investigate the initial stages of bimetallic cluster formation including metal–metal bond formation in supported clusters. We began with small, well-defined reactive monometallic precursors, $[Os_3(CO)_{12}]$ and $[Ru_3(CO)_{12}]$, to maximize the opportunity to understand details of the chemistry. These precursors also offer the advantages that their chemistry on oxide surfaces and their decarbonylation chemistry are relatively well understood,[5–7] and the bimetallic carbonyl clusters are known.[8] Our strategy was to adsorb the two precursors intact on a high-area support (MgO), so that the activation by decarbonylation and Ru–Os bond formation could be followed in real time with infrared (IR) spectroscopy to characterize the ligands and with extended X-ray absorption fine structure (EXAFS) spectroscopy to characterize the ligands and the metal–metal bonds as they were formed. We stress the importance of measuring EXAFS spectra at two metal edges:[9] the criteria for demonstrating the internal consistency of the data at the two edges are essential in the EXAFS data fitting and provide a stronger assurance of the validity of the fits than in the case of monometallics.[*]

The results demonstrate that $[Ru_3(CO)_{12}]$ on high-area MgO powder in the presence of $H_2$ underwent partial decarbonylation and aggregation of the metal, and as the sample was treated at higher temperatures, $[Os_3(CO)_{12}]$ also underwent partial decarbonylation—and the formation of Ru–Os bonds ensued.

All experiments were done with samples in flow reactor cells, one for IR and one for EXAFS experiments. The gas-phase products were analyzed by mass spectrometry. IR spectra of the initially prepared sample in flowing helium indicate the presence of segregated triruthenium carbonyl clusters and triosmium carbonyl clusters on the MgO. The $\nu_{CO}$ region of the spectrum characterizing the adsorbed species includes bands at 2052(vs) and 1960(s), consistent with adsorbed $[Ru_3(CO)_{12}]$,[10] and bands at 2075(vs), 2019 (s), 2006(vs), and 1950(w) $cm^{-1}$, consistent with reports[5] indicating the adsorption of $[Os_3(CO)_{12}]$ to form $[Os_3(CO)_{11}]^{2-}$ ion-paired with $Mg^{2+}$ sites on the MgO surface (referred to as $[Os_3(CO)_{11}]^{2-}$/MgO).

Consistent with these data, EXAFS spectra of the initially prepared sample obtained at the Ru K edge indicate the lack of Ru–Os contributions, confirming the presence of only monometallic supported species. Similarly, Os $L_{III}$ edge indicate no Os–Ru contribution. The EXAFS data indicate a Ru–Ru coordination number ($N_{Ru-Ru}$) of $1.9 \pm 0.4$ at a distance of $2.90 \pm 0.02$ Å, indicative of triruthenium clusters, and an Os–Os coordination number ($N_{Os-Os}$) of $2.1 \pm 0.4$ at a distance of $2.89 \pm 0.02$ Å, consistent with earlier results[5] and triosmium clusters. The EXAFS data also give evidence of metal–support interactions and the presence of carbonyl ligands on the metals (Supporting Information, Tables SI-1 and 2). Specifically, the EXAFS data indicate that, on

[*] A. Kulkarni, Prof. B. C. Gates
Department of Chemical Engineering and Materials Science
University of California
One Shields Avenue, Davis, CA 95616 (USA)
Fax: (+1) 530-752-1031
E-mail: bcgates@ucdavis.edu
Homepage: http://www.chms.ucdavis.edu/research/web/catalysis

[**] This work was supported by the National Science Foundation, GOALI Grant CTS-05-00511, and ExxonMobil. We acknowledge beam time and support of the DOE Division of Materials Sciences for its role in the operation and development of beam line MR-CAT at the Advanced Photon Source at Argonne National Laboratory.

Supporting information for this article is available on the WWW under http://dx.doi.org/10.1002/anie.200904877.

[*] The parameters determined from each edge and characterizing the bimetallic (Ru–Os and Os–Ru) interactions must have a) the same bond distances and b) the same Debye–Waller factors; furthermore, c) the coordination numbers characterizing the interactions between atoms of different metals and determined from data at each absorption edge must be related to each other by the equation $N_{Os-Ru}/N_{Ru-Os} = n_{Ru}/n_{Os}$, where $n_{Ru}$ and $n_{Os}$ are the total numbers of Ru and Os atoms in the sample, respectively.[9]

average, each Ru atom was bonded to two other Ru atoms, four carbonyl ligands, and one support oxygen, and each Os atom on average was bonded to two other Os atoms, four carbonyl ligands, and one support oxygen atom. Details are given in the Supporting Information with a summary of the errors.

When the gas flow was switched from helium to $H_2$ at room temperature, no change in either the IR or EXAFS spectrum was evident, but when the temperature was raised to 423 K at 1.5 K min$^{-1}$ with the $H_2$ flow continuing at 1 bar, the metal ligand environments changed. IR spectra (Figure 1) taken during the temperature ramp show the removal of CO ligands. Peaks (2052 and 1960 cm$^{-1}$) attributed to triruthenium carbonyl clusters first started to decrease in intensity at approximately 333 K, whereas the peaks attributed to triosmium carbonyl clusters (2075, 2019, 2006, and 1950 cm$^{-1}$) began to decrease in intensity at 358 K. The IR spectra of the supported sample after the treatment in $H_2$ at 423 K include $\nu_{CO}$ peaks at 2043, 2030, 2010, 1994, 1958, and 1942 cm$^{-1}$ that are similar to those of $[H_2Os_3Ru(CO)_{13}]$,[5] suggesting the onset of bimetallic cluster formation (but not being sufficient to determine the structure).

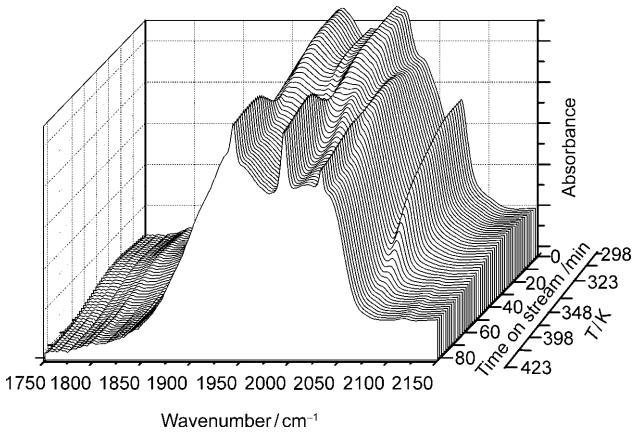


***Figure 1.*** Removal of CO ligands from the supported clusters: $\nu_{CO}$ region of IR spectra recorded at 1 min intervals during $H_2$ flow as the temperature increased from 298 to 423 K at 1.5 K min$^{-1}$.

To bolster the IR evidence of bimetallic cluster formation, we used EXAFS spectroscopy to track the formation of Ru–Os bonds as the temperature was ramped to 423 K at 1.5 K min$^{-1}$ with the sample in flowing $H_2$ at 1 bar (Figure 2). X-ray absorption near edge (XANES) spectra recorded at the Ru K edge and at the Os $L_{III}$ edge show changes in the environments of the metal atoms (Figure 3); the isosbestic points indicate the transformation of one species to another (Figure 3 shows the data at the Ru K edge; data obtained at the Os $L_{III}$ edge are shown in the Supporting Information). The XANES spectra clearly demonstrate that the supported species that were formed were different from the initial supported metal–carbonyl clusters (and from the respective metal foils).

EXAFS spectra recorded at the Ru K edge during this treatment show a decrease in the Ru–C and Ru–O* coordination numbers (O* is the oxygen of CO ligands,

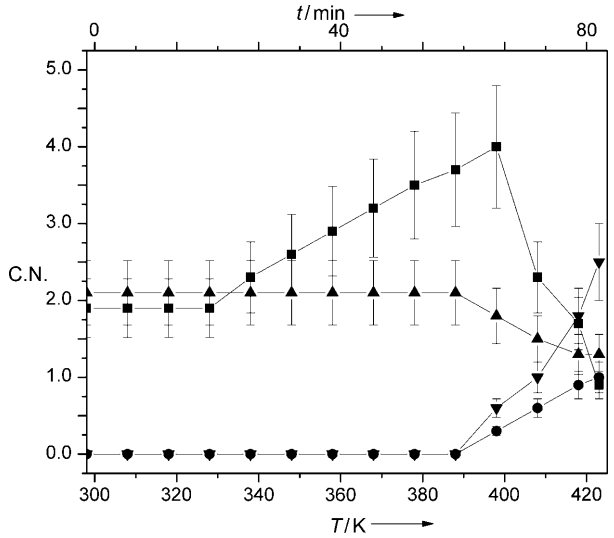


***Figure 2.*** EXAFS data characterizing change in coordination numbers (C.N.) of the supported bimetallic sample in flowing $H_2$ as the temperature increased from 298 to 423 K (at 1.5 K min$^{-1}$) at 1 bar. ■ Ru–Ru, ● Ru–Os, ▲ Os–Os, ▼ Os–Ru.

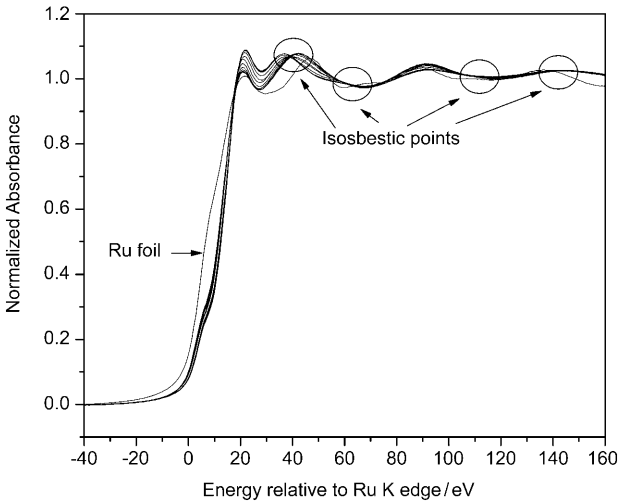


***Figure 3.*** Normalized XANES spectra at the Ru K edge of the sample during the cluster formation as the temperature was ramped from 298 to 423 K (at 1.5 K min$^{-1}$) in $H_2$ flow at 1 bar.

distinguished by multiple scattering in linear Ru-C-O moieties), indicating the onset of decarbonylation of the triruthenium clusters at 333 K, in agreement with the IR results. Over the temperature range of 333–398 K the Ru–C and Ru–O* coordination numbers decreased from $4.0 \pm 0.8$ and $3.8 \pm 0.8$ to $2.6 \pm 0.5$ and $2.3 \pm 0.5$, respectively, indicating the degree of partial decarbonylation. Simultaneously, the $N_{Ru-Ru}$ increased from 1.9 to 4.0, indicating aggregation of the ruthenium into larger clusters. This aggregation was accompanied, as expected, by a decrease in the $Ru-O_{support}$ coordination number (Table SI-3). There was no EXAFS evidence of Ru–Os contributions in this range of treatment temperature.

In summary, the data obtained in the temperature range of 333–398 K demonstrate the breaking of Ru–CO bonds,

  

generating coordinative unsaturation of the ruthenium, and formation of Ru–Ru bonds, which required breaking of Ru–$O_{support}$ bonds and migration of Ru atoms.

The Ru–Ru distance characterizing the sample treated at 398 K as the clusters were being further decarbonylated was 0.06 Å greater than the value characterizing the initially adsorbed triruthenium clusters (Table SI-3); these results suggest the beginning of Ru–Ru bond breaking.

At temperatures above 398 K, the EXAFS Ru K edge data demonstrate the appearance of a new Ru–Os contribution, at a distance of 2.78 Å. $N_{Ru-Ru}$ decreased as the temperature increased further. When the temperature reached 423 K, $N_{Ru-Ru}$ had decreased to 0.9, and the Ru–Os coordination number had increased to 1 (Figure 2, Table SI-3).

EXAFS spectra recorded at the Os $L_{III}$ edge during this treatment show a decrease in the Os–C and Os–O* contributions, with the onset of decarbonylation of the triosmium clusters being evident at 360 K, consistent with the IR results. As the temperature increased from 360 to 398 K, the Os–C and Os–O* coordination numbers decreased from $4.0 \pm 0.8$ and $4.1 \pm 0.8$ to $2.8 \pm 0.6$ and $2.7 \pm 0.5$, respectively, indicating partial decarbonylation of the osmium, but no change in $N_{Os-Os}$ was observed, which indicates the retention of the triosmium frame.

As the temperature reached 398 K, a new contribution—attributed to Os–Ru bonds—appeared, indicating the inception of bimetallic cluster formation, reinforcing the result shown by the Ru K edge data. At temperatures above 398 K, the Os–Ru coordination number continued to increase with a concomitant decrease in the $N_{Os-Os}$, demonstrating increasing bimetallic cluster formation (Figure 2, Table SI-4).

The IR and EXAFS spectra taken together provide the foundation for a model of the chemistry of the supported bimetallic cluster formation (Figure 4), involving, first, the decarbonylation of triruthenium clusters starting at 333 K (with the triosmium carbonyl clusters still being coordinatively saturated and intact). The coordinatively unsaturated ruthenium species were reactive, and, at 333 K, had aggregated substantially so that the average ruthenium cluster was larger than triruthenium (and the EXAFS data provide a basis for an approximate model of the average cluster, Figure 4). When the temperature had been raised to about 358 K, the triosmium clusters began to undergo decarbonylation, and at approximately 398 K the triosmium clusters had lost enough CO ligands to become sufficiently coordinatively unsaturated to allow migration and reaction with Ru atoms of neighboring species. Thus, the data clearly delineate the separate steps in the bimetallic cluster synthesis (Figures 2 and 4).

We stress that mixtures of surface species were present on the MgO as the bimetallic cluster synthesis took place. For example, the Ru–Ru contributions did not disappear in our experiments, a result that suggests that not all of the triruthenium clusters had been converted. A similar statement pertains to the osmium clusters. Thus, it is clear that the sample containing the bimetallic clusters also contained monometallic species (i.e., those containing only one kind of metal atom, Ru or Os), and they were of various nuclearities, as evidenced by the increased Ru–Ru coordination numbers. Thus, our data are not sufficient to determine the populations of the bimetallic and the monometallic clusters. Such information might be attainable by high-resolution transmission electron microscopy (TEM), but, so far, TEM data providing such fine-grained detail are lacking.

The novelty of this work is the evidence of how bimetallic clusters are formed, with a resolution of the stages of formation of coordinative unsaturation followed by migration of metals and formation of metal–metal bonds. We stress the value of characterization of the samples by EXAFS spectroscopy at two metal edges and the importance of IR spectroscopy in characterization of the ligands to complement the EXAFS data.

## Experimental Section

MgO powder (EM Science, surface area 70 $m^2 g^{-1}$) was calcined in $O_2$ at 673 K for 6 h and evacuated at 673 K for 14 h, isolated, and stored in an argon-filled glovebox with less than 1 ppm $O_2$ and water. The precursors $[Os_3(CO)_{12}]$ and $[Ru_3(CO)_{12}]$ reacted with the treated MgO in a slurry in dried, deoxygenated *n*-pentane at 298 K. The Ru and Os contents of the resultant powders were each 1.0 wt%.

Time-resolved X-ray absorption spectra were recorded at X-ray beamline MR-CAT at the Advanced Photon Source at Argonne National Laboratory. The storage ring electron energy and ring currents were 7.0 GeV and 105 mA, respectively. The cryogenic double-crystal Si(111) monochromator was detuned by 20–25% at the Ru K and Os $L_{III}$ edges to minimize the effects of higher harmonics in the X-ray beam. In an argon-filled glove box, powder samples were loaded into a flow-through cell, which was sealed in the inert atmosphere. The mass of each sample was chosen for optimal absorption measurements at the Ru K edge (22117 eV) and the Os $L_{III}$ edge (10871 eV), giving an X-ray absorbance of approximately 2.5 calculated at an energy 50 eV greater than the absorption edge. Data were recorded at 1 bar and temperatures between 298 and 423 K in transmission mode for 3.5 min to determine each spectrum; this time represents a compromise between data quality and frequency of data collection for good time resolution.

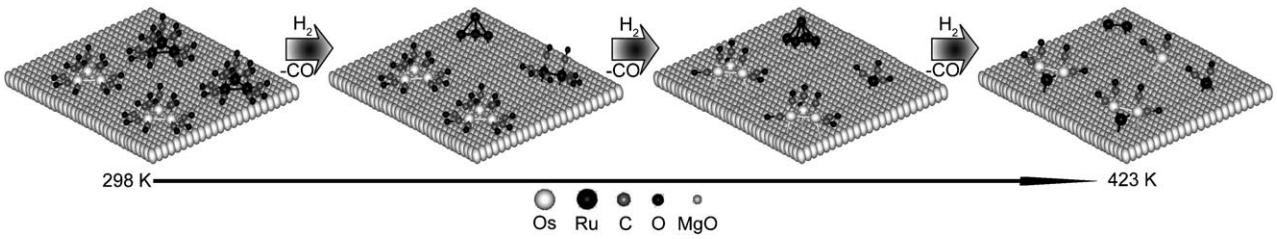


***Figure 4.*** Model of bimetallic cluster formation in $H_2$ as the temperature increased from 298 to 423 at 1.5 K $min^{-1}$. Structures were constructed on the basis of EXAFS and IR results and are simplified.

  

The data fitting was done with the Sinfelt criterion[9] as an internal consistency check.

More details and other methods are described in the Supporting Information and the references cited therein.

Received: September 1, 2009
Published online: November 24, 2009

**Keywords:** bimetallic clusters · carbonyl ligands · cluster formation · decarbonylation · time-resolved spectroscopy

[1] J. H. Sinfelt, *Bimetallic Catalysts: Discoveries, Concepts, and Applications*, Wiley, New York, **1983**.
[2] O. S. Alexeev, B. C. Gates, *Ind. Eng. Chem. Res.* **2003**, *42*, 1571.
[3] J. D. Aiken, R. G. Finke, *J. Mol. Catal.* **1999**, *145*, 1.
[4] A. Uzun, B. C. Gates, *Angew. Chem.* **2008**, *120*, 9385; *Angew. Chem. Int. Ed.* **2008**, *47*, 9245.
[5] V. A. Bhirud, H. Iddir, N. D. Browning, B. C. Gates, *J. Phys. Chem. B* **2005**, *109*, 12738.
[6] R. Ugo, C. Dossi, R. Psaro, *J. Mol. Catal.* **1996**, *107*, 13.
[7] R. Psaro, C. Dossi, R. Ugo, *J. Mol. Catal.* **1983**, *21*, 33.
[8] J. R. Budge, J. P. Scott, B. C. Gates, *J. Chem. Soc. Chem. Commun.* **1983**, 342.
[9] G. H. Via, K. F. Drake, G. Meitzner, F. W. Lytle, J. H. Sinfelt, *Catal. Lett.* **1990**, *5*, 25.
[10] G. Shen, A. M. Liu, M. Ichikawa, *J. Chem. Soc. Faraday Trans.* **1998**, *94*, 1353.

  